A Top-Down Cortical Circuit for Accurate Sensory Perception

Highlights

- Somatosensory (S1) and secondary motor (M2) cortices form a top-down circuit

- Sensory stimulation induces sequential S1 to M2 and M2 to S1 input patterns

- M2 evokes a dendritic spike and persistent firing in S1 layer 5 (L5) neurons

- Optogenetic inhibition of M2 to S1 axons degrades accurate sensory perception

Authors

Satoshi Manita, Takayuki Suzuki, ...,
Matthew E. Larkum,
Masanori Murayama

Correspondence

masa_murayama@brain.riken.jp

In Brief

Top-down input from higher brain areas to primary sensory areas is thought to merely modulate perception. Using a multidisciplinary approach in mice, Manita et al. demonstrate that top-down input is essential for accurate perception.

CrossMark

CellPress

A Top-Down Cortical Circuit
for Accurate Sensory Perception

Satoshi Manita,[1,10] Takayuki Suzuki,[1,10] Chihiro Homma,[1] Takashi Matsumoto,[1] Maya Odagawa,[1] Kazuyuki Yamada,[1] Keisuke Ota,[1,2] Chie Matsubara,[1] Ayumu Inutsuka,[3] Masaaki Sato,[4,5] Masamichi Ohkura,[6,7] Akihiro Yamanaka,[3] Yuchio Yanagawa,[8] Junichi Nakai,[6,7] Yasunori Hayashi,[4,6,7] Matthew E. Larkum,[9] and Masanori Murayama[1,*]

[1]Laboratory for Behavioral Neurophysiology, Brain Science Institute, RIKEN, 2-1 Hirosawa, Wako City, Saitama, 351-0198, Japan
[2]JSPS Research Fellow, 5-3-1 Kojimachi, Chiyoda-ku, Tokyo, 102-0083, Japan
[3]Department of Neuroscience II, Research Institute of Environmental Medicine, Nagoya University, Furocho, Chikusa-ku, Nagoya City, Aichi, 464-8601, Japan
[4]Brain Science Institute, RIKEN, 2-1 Hirosawa, Wako City, Saitama, 351-0198, Japan
[5]PRESTO, Japan Science and Technology Agency, 4-1-8 Honmachi, Kawaguchi City, Saitama, 332-0012, Japan
[6]Saitama University Graduate School of Science and Engineering, 255 Shimo-Okubo, Sakura-ku, Saitama City, Saitama, 338-8570, Japan
[7]Saitama University Brain Science Institute, 255 Shimo-Okubo, Sakura-ku, Saitama City, Saitama, 338-8570, Japan
[8]Department of Genetic and Behavioral Neuroscience, Gunma University Graduate School of Medicine, 3-39-22 Showa-machi, Maebashi City, Gunma, 371-8511, Japan
[9]NeuroCure Cluster of Excellence, Humboldt University, Charitéplatz 1, D-10117 Berlin, Germany
[10]Co-first author
*Correspondence: masa_murayama@brain.riken.jp
http://dx.doi.org/10.1016/j.neuron.2015.05.006

SUMMARY

A fundamental issue in cortical processing of sensory information is whether top-down control circuits from higher brain areas to primary sensory areas not only modulate but actively engage in perception. Here, we report the identification of a neural circuit for top-down control in the mouse somatosensory system. The circuit consisted of a long-range reciprocal projection between M2 secondary motor cortex and S1 primary somatosensory cortex. In vivo physiological recordings revealed that sensory stimulation induced sequential S1 to M2 followed by M2 to S1 neural activity. The top-down projection from M2 to S1 initiated dendritic spikes and persistent firing of S1 layer 5 (L5) neurons. Optogenetic inhibition of M2 input to S1 decreased L5 firing and the accurate perception of tactile surfaces. These findings demonstrate that recurrent input to sensory areas is essential for accurate perception and provide a physiological model for one type of top-down control circuit.

INTRODUCTION

The capacity for complex behavior requires top-down control (Mesulam, 1998; Miller and Cohen, 2001). In physiological terms, top-down control is defined as the regulation by higher brain areas (i.e., top) of neuronal activity and information processing in lower brain areas (i.e., bottom). Hence, top-down control serves to modulate the neural signals from bottom-up sensory input to refine behavior as a function of an animal's goal orientation. This regulation can be as simple as the refinement of sensory experience or as complex as executive control of a behavioral program. Given the diverse perceptual and cognitive behaviors governed by top-down control, the range of associated neural signals is vast, including attention, value, and memory (Corbetta and Shulman, 2002; Meyer, 2011; Tomita et al., 1999; Zanto et al., 2011). Thus, top-down control is a major component of complex behavior and in neural systems implementing cognition (Dehaene et al., 2006; Gilbert and Sigman, 2007).

Despite the fundamental role of top-down control in animal behavior, the anatomical structure and physiological mechanisms of the responsible neural circuits remain unclear. Anatomically, top-down signals are presumed in mammals to use long-range intracortical horizontal projections between higher and lower brain areas (Cauller et al., 1998; Felleman and Van Essen, 1991; Johnson and Burkhalter, 1996). In one example, bottom-up sensory input typically evokes an early and late activity component in primary sensory areas. The late component is believed to involve top-down control and correlate with conscious perception (Del Cul et al., 2007). Kulics and colleagues described touch stimulus responses in monkey (Cauller, 1995; Cauller and Kulics, 1988; Kulics, 1982; Kulics et al., 1977) and found that the early component correlates with stimulus intensity related to thalamic input and the late component with behavioral responses. Consistent with these findings, during a whisker-stimulation detection task, inhibition of the late component in barrel cortex correlated with suppression of behavior (Sachidhanandam et al., 2013). Collectively, these data suggest a potential link between the late component of cortical activity and top-down control, but the functional and anatomical neural circuit architecture of the late component remains poorly defined.

There are several potential sources of top-down input to S1 primary somatosensory cortex, including motor cortex (Petreanu et al., 2012; Xu et al., 2012), secondary somatosensory cortex (S2) (Cauller et al., 1998), and second-order thalamic nuclei (Rubio-Garrido et al., 2009). According to current models of cortical processing in sensory perception, prefrontal cortical areas receive bottom-up neural signals from primary sensory areas and return feedback to the sensory areas (Gilbert and Sigman, 2007; Lamme, 2001; Olson et al., 2001; Tomita et al., 1999; Zanto et al., 2011), although this arrangement remains conjecture (Gilbert and Sigman, 2007). Among prefrontal cortical areas governing top-down input to somatosensory cortex, secondary motor cortex, called M2, is well positioned. In rodent, motor cortex is divided into primary motor cortex (M1) for direct motor control and located adjacent to S1 and the more rostral M2 (Neafsey et al., 1986), also called medial agranular cortex (AGm), that is linked to higher brain functions including value-based decision making (Sul et al., 2011) and self-initiated action (Murakami et al., 2014). There is indirect evidence that M2 may transmit top-down information to control sensory perception where corollary discharge, an efferent copy of motor input from M2 to sensory cortices, is hypothesized to modulate perception (Schneider et al., 2014). Moreover, lesions of M2 can produce somatosensation neglect in rodents (Vargo et al., 1988), consistent with anatomical data showing reciprocal anatomical connectivity between S1 and M2 (Neafsey et al., 1986; Reep et al., 1984, 1987, 1990). Despite this circumstantial evidence, the causal identification of a horizontal circuit from M2 to S1, and whether M2 input is responsible for sensory stimulus-evoked late activity in S1, is unknown. In more general terms, it remains unclear in any sensory system whether top-down projections innervating sensory areas merely modulate perception or are fundamentally involved in perception.

In this study, we identify and characterize a top-down control circuit in the mouse somatosensory system. Using wide-field voltage-sensitive dye imaging during somatosensory hindpaw stimulation, we identified a functional top-down projection between M2 and S1 with early and late activity components. The middle anterior part of the hindpaw somatosensory area overlaps with hindpaw primary motor area (M1) in rodents (Ayling et al., 2009). However, in this study we define S1 based on recorded neural activity from a lateral posterior part of the hindpaw area where L4 exists and neural activity correlated with sensory input, as well as in the forepaw area (Milenkovic et al., 2014). We studied the anatomical projection from M2 to S1 and measured physiological signals in S1 during hindpaw stimulation using viral tracing and multiunit recordings, respectively. We found that top-down signals to both the upper and lower layers of S1 correlate with sustained dendritic activity in S1 layer 5 (L5) pyramidal neurons. Two-photon dendritic calcium (Ca^{2+}) imaging and multiunit recordings from these neurons indicated that L5 dendritic activity promotes efficient cortical output. Finally, optogenetic inactivation of the top-down projection from M2 to S1 demonstrated that top-down input does not merely modulate perception but can have a direct role in the formation of accurate somatosensory perception.

RESULTS

Identification of a Top-Down Cortical Circuit

During mouse hindpaw stimulation, we used wide-field cortical voltage-sensitive dye (cVSD) imaging (Ferezou et al., 2007) (Figure 1A) to search for a reciprocal functional connection between S1 (hindpaw area; hereafter called S1) and M2 (Neafsey et al., 1986; Reep et al., 1984, 1987; Reep et al., 1990) associated with somatosensory perception. Under anesthesia, a mild electrical stimulation (single pulse, 0.1 ms duration, 100 V) of the hindpaw evoked early neural activity in S1 followed by a subsequent response in an anterior medial area often referred to as AGm (Figure 1B) (Neafsey et al., 1986; Reep et al., 1990) and also known in mice as the secondary motor area (M2) (Paxinos and Watson, 1998). The location of this area could be distinguished from forepaw M2 via forepaw stimulation, and from vibrissal primary and secondary motor cortices (vM1 and vM2) (see Figure S1 available online), indicating somatotopic map within M2, analogous to S1 and M1. Next we examined whether M2 and S1 form a functional connection using a sodium channel blocker, tetrodotoxin (TTX, 3 μM), or an AMPA/kainate receptor blocker, CNQX (100 μM), applied to either S1 or M2 during hindpaw stimulation under anesthesia. The pharmacological inactivation of S1 decreased the early component of cVSD activity in M2 (Figures 1D and 1H), and the inactivation of M2 decreased the late component of cVSD activity in S1 (Figures 1I and 1M). Together, these findings suggest that M2 and S1 form a reciprocal circuit that may be involved in somatosensory processing.

Previous studies indicated that top-down corticocortical projections from higher areas to primary areas generally terminate in the upper and lower layers, whereas bottom-up feedforward projections terminate primarily in the middle layers (Cauller, 1995; Coogan and Burkhalter, 1990; Felleman and Van Essen, 1991; Ueta et al., 2013). To confirm these axonal projections, we used anterograde viral tracing to examine the anatomical connectivity between S1 and M2. An adeno-associated viral tracer carrying green fluorescent protein (GFP) with a CAG-driven promoter, AAV-CAG-GFP (AAV-GFP), was injected into either S1 or M2 to anterogradely label axons (Figures S2A and S3A), and the retrograde tracer cholera toxin subunit B (CT-B) conjugated to Alexa 555 was used to label the somata of projection neurons (Figures S2F and S3D). The M2 axonal innervation pattern estimated from fluorescence density and total intensity showed targeting to layer 1 (L1) and deep cortical layers, with less in the middle layers (Figures S2B–S2E and S2I), suggestive of previously described top-down connections. Boutons from M2 axons were also observed in all layers (Figure S2E). L2/3, L5a, and L6 neurons in M2 sent their axons to S1 (Figures S2G–S2I), similar to a top-down projection from M2 to M1 (Ueta et al., 2013). Reverse tracing experiments (i.e., AAV-GFP in S1 and CT-B in M2) revealed a predominance of projecting neurons from layers 2/3, 5a, and lower layer 6 of S1 to M2 (Figure S3) that terminated in a feedforward (bottom-up) connectivity pattern (Coogan and Burkhalter, 1990; Felleman and Van Essen, 1991). We confirmed that these long-range projections consisted of calcium/calmodulin-dependent protein kinase II (CaMKII)-positive excitatory neurons by using glutamate
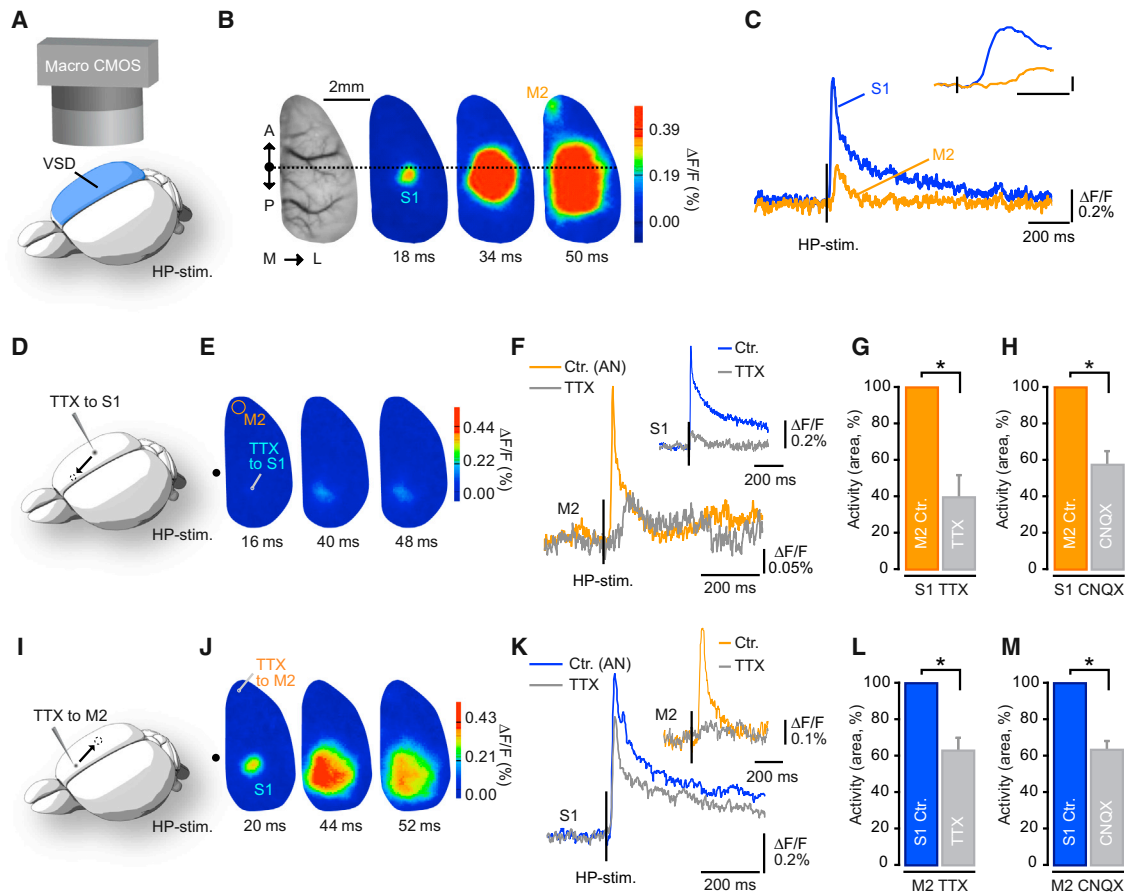
Figure 1. Identification of a Reciprocal Top-Down Control Circuit

(A) Diagram showing macroscopic recording of cortical activity by using voltage-sensitive dye (cVSD) imaging.

(B) Spatiotemporal dynamics of cVSD response evoked by hindpaw (HP) stimulation (single pulse, 0.1 ms duration, 100V) under anesthesia. Time after stimulation is indicated. A, anterior; P, posterior; M, middle; L, lateral; S1, hindpaw area of the primary somatosensory cortex; M2, hindpaw area of the secondary motor cortex.

(C) Cortical activity traces. Inset, expanded traces. Vertical axis, 0.2% ΔF/F. Horizontal axis, 30 ms.

(D) Experimental diagram. TTX was applied locally to S1. Cortical activity was evoked by hindpaw stimulation under anesthesia.

(E) Examples of spatiotemporal dynamics of cVSD response.

(F) M2 (orange) and S1 activities (inset, blue) before and after TTX application.

(G) Summary of (F) (40.7% ± 12.3% of control, n = 8 mice, t_7 = 4.82, *p < 0.05, Student's paired t test).

(H) Summary of M2 activity after local application of CNQX to S1 (56.6% ± 7.9% of control, n = 6 mice, t_5 = 5.50, *p < 0.01, Student's paired t test).

(I) Experimental diagram. TTX was applied locally to M2. Cortical activity was evoked by hindpaw stimulation under anesthesia.

(J) Examples of the spatiotemporal dynamics of cVSD responses.

(K) S1 and M2 activities (inset) before and after TTX application.

(L) Summary of (K) (64.6% ± 7.0% of control, n = 8 mice, t_7 = 5.02, *p < 0.05, Student's paired t test).

(M) Summary of S1 activity after local application of CNQX to M2 (63.4% ± 4.5% of control, n = 6 mice, t_5 = 8.08, *p < 0.01, Student's paired t test). Data are represented as mean ± SEM. See also Figures S1–S4.

---

decarboxylase 67-green fluorescent protein (GAD67-GFP) knock-in mice to label inhibitory neurons (Figure S4) (Tamamaki et al., 2003).

Functional M2 Projection to S1 Upper and Lower Layers

Anatomically, the M2 axonal projection pattern to S1 indicated termination in upper and lower layers. To examine the functional M2 to S1 projection, we performed multiunit recordings (MUR) from all layers of S1 using a vertical array of up to 16 electrodes (Michigan Probes) during hindpaw stimulation (Figure 2). After

hindpaw stimulation under anesthesia, we observed action potential (AP) activity in S1, with two peaks occurring early at ~23 ms and late ~110 ms in L5 (Figures 2A–2C). Although more physiological stimulation (air puff) to the hindpaw also induced the firing activity including two or more components (Figure S5A), we used the same mild electrical stimulation protocol throughout the study for precise control of stimulus intensity. APs were first detected in the middle layer (L4, 300–400 μm below the cortical surface), consistent with bottom-up thalamic input (Figure 2B, top) (Armstrong-James et al., 1992;
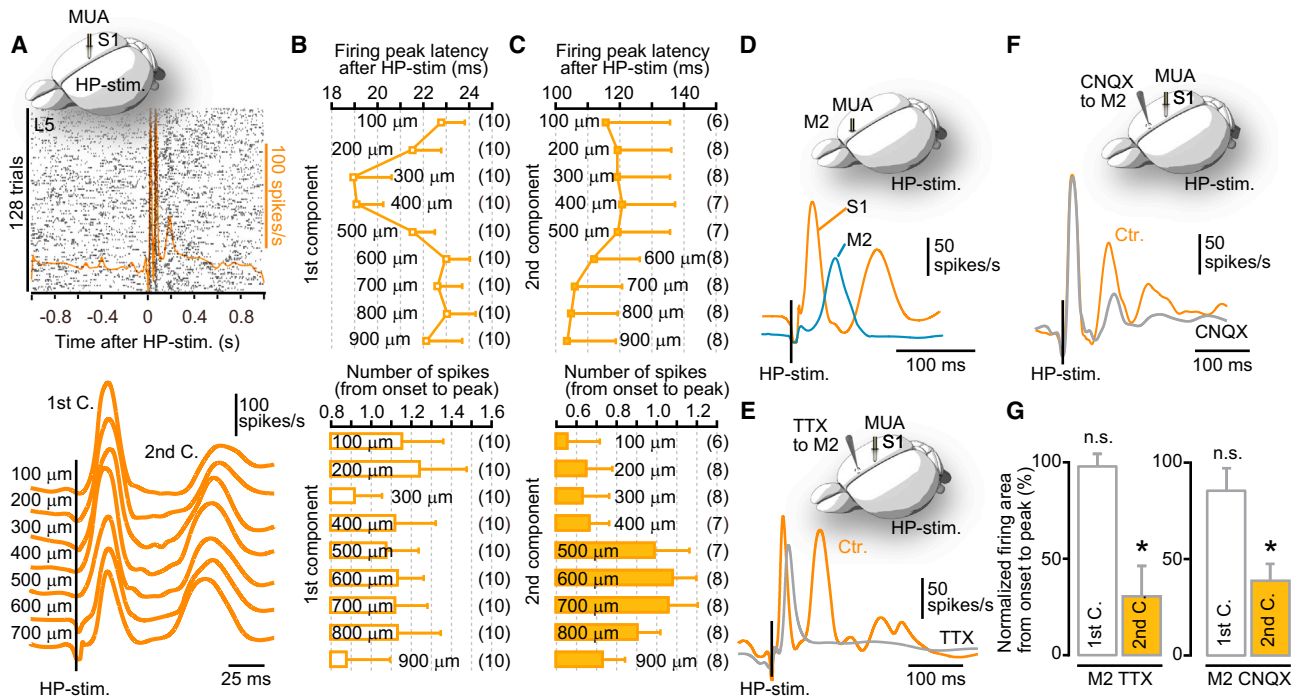
Figure 2. Top-Down Input Activates a Late Response in Somatosensory Cortex

(A) Top, multiunit activity (MUA) evoked by hindpaw stimulation (single pulse, 0.1 ms duration, 100 V) was recorded from S1 (inset) under anesthesia. Raster plots show the MUA recorded 600 μm below the cortical surface across 128 trials. The orange line indicates the estimated spike rates. Hindpaw stimulation was applied at 0 ms. Bottom, the estimated spike rates recorded from seven sites. The vertical black lines indicate the time of stimulation. Note the decreased spike rate around the hindpaw stimulation due to stimulation artifact.

(B) The latency (top) and number of spikes (bottom) of the first peak (component).

(C) The latency (top) and number of spikes (bottom) of the second peak (component).

(D) The MUA evoked by hindpaw stimulation was recorded from M2 (600–700 μm below the surface, blue), which peaked during the first and second components of the S1 (orange).

(E) S1 firing activity (600 μm below the surface) before (orange) and after (gray) TTX application to M2 (see also Figure S5 for other layers).

(F) S1 firing activity (600 μm below the surface) before (orange) and after (gray) CNQX application to M2.

(G) Summary of the TTX and CNQX effects on the first and second components of the estimated spike rate (each experiment, n = 11 mice for TTX experiment, n = 6 mice for CNQX experiment; TTX, $t_{10} = -4.45$; CNQX, $t_5 = 7.05$, *p < 0.05, Student's paired t test). The numbers in parentheses show the numbers of mice used in each experiment. Data are represented as mean ± SEM; n.s., not significant.

Constantinople and Bruno, 2013), followed within ∼4 ms by APs in other cortical layers that indicated general activation of the entire cortical column (Figure 2B, bottom). Notably, the propagation of the late activity component was sequential, starting in lower layers followed by upper layers (Figure 2C, top). Hindpaw stimulation evoked AP activity in S1 L5 during the late component and only sparsely in the other layers (upper layers and L6) (Figure 2C, bottom). We next asked whether the late S1 L5 activity was due to the influence of M2 activity as suggested by our cortical VSD imaging data which indicated that the late S1 response was dependent on M2 (Figures 1K–1M).

To examine the source of the S1 late activity, we performed MUR in M2 and found that the average peak latency for firing in L5 of M2 was 80.0 ± 6.0 ms (n = 4 mice, Figure 2D), indicating an intermediate time between the early and late components recorded in S1. We further examined how M2 influenced the two activity phases in S1 by injecting TTX or CNQX into M2 and recording from S1 during hindpaw stimulation (Figures 2E–2G). The inactivation of M2 had no effect on the early component

but caused a marked decrease in the late component in all layers, especially L5 of S1 (Figures 2E–2G; see Figures S5B–S5D for a summary of other layers and for TTX injection to visual cortex as a control experiment). These experiments also indicated that drug application to M2 did not directly affect the recording site in S1. Our results demonstrated that M2 firing and synaptic activity are necessary for L5 firing in S1 during the hindpaw stimulation-evoked late component. This M2-required L5 firing is, however, inconsistent with the M2 axon projection that targets mainly L6 and L1 of S1.

The apparent inconsistency may result from a large synaptic input from M2 to L5 of S1, not evident from the anatomical data. To understand the pattern and strength of M2 synaptic input to S1, we performed current source density (CSD) analysis with linear probes during hindpaw stimulation (Figures 3A–3C). Similar to the observed AP activity, we also found two components of synaptic input (defined as current sinks). The first sink activity observed at L4 was consistent with thalamic input (Figure 3D). Notably, we found that although L5 dominated spike
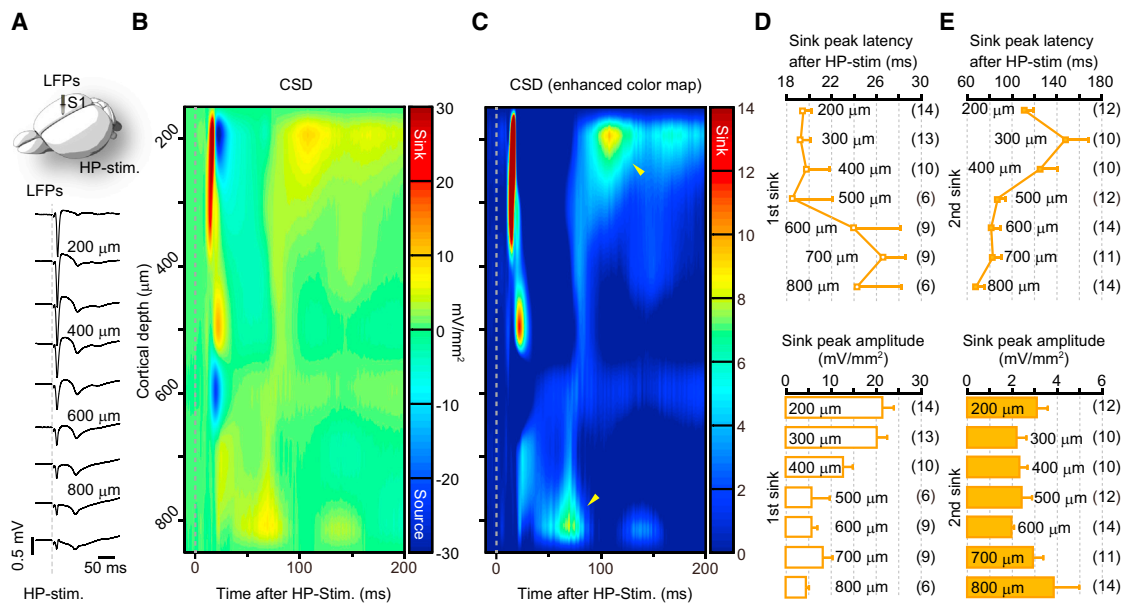
Figure 3. Top-Down Input Activates the Lower and Upper Layers of S1

(A) Top, local field potentials (LFPs) induced by hindpaw stimulation (single pulse, 0.1 ms duration, 100 V) were measured in S1 under anesthesia. Bottom, examples of the LFPs recorded at different depths. The vertical line indicates hindpaw stimulation timing (gray dotted line). Note that stimulus artifacts were removed for clarity.

(B) Example of a current source density (CSD) profile as a color image plot in response to mouse hindpaw stimulation.

(C) Enhanced color map of (B). Arrowheads indicate sink activity during the second sink.

(D) The latency (top) and peak amplitude (bottom) of sink activity during the first sink.

(E) The latency (top) and peak amplitude of sink activity (bottom) during the second sink. The numbers in parentheses show the numbers of mice used in each experiment. Data are represented as mean ± SEM.

activity (Figure 2C, bottom), sinks corresponding to the late component were found in the lower and upper layers (Figure 3E), consistent with the anatomical tracing data. The averaged overlap period of sinks between 800 μm and 200 μm below from the cortical surface was ∼30 ms (n = 8; Figure S5E). To examine if the lower and upper layer sink activity was due to M2 synaptic input, we used M2 intracortical microstimulation (ICMS) or hindpaw stimulation before and after application of CNQX to the S1 cortical surface (Figure S5F). S1 sink activity was significantly blocked by CNQX application, indicating a dependence on M2 synaptic activity.

M2 Synaptic Control of the S1 L5 Dendritic Spike

Our CSD data (Figure 3E, bottom) suggested that more M2 synaptic input arrives at the lower (L6) and upper layers (L1 and L2/3) than at L5, consistent with the anatomical data. However, this finding was inconsistent with the multiunit data indicating the highest firing activity in L5 (Figure 2C, bottom). One explanation for this inconsistency was that synaptic input to the lower and upper layers caused local Ca²⁺ spikes in L5 apical dendrites and increased firing in L5 neurons (Larkum et al., 1999; Xu et al., 2012). To examine this hypothesis, we measured Ca²⁺ activity in single dendrites of L5 pyramidal neurons. Using a transgenic mouse line in which layer 5 pyramidal neurons express the GECI (genetically encoded Ca²⁺ indicator) G-CaMP7 (Ohkura et al., 2012; Sato et al., 2013), we performed two-photon imaging of distal apical dendritic Ca²⁺ activity ∼200 μm below the cortical

surface under anesthesia before and after CNQX injection to M2 (Figures 4A and 4B). Before CNQX application, hindpaw stimulation evoked dendritic activity with either early and small dendritic activity (Figure 4C, light blue arrowhead), followed by late and large activity (Figure 4C, deep blue arrowhead). After CNQX application to M2, the large but not the small component was blocked (Figures 4C and 4D), indicating that the late and large dendritic activity observed S1 L5 neurons required activity from the M2 projection.

We further studied cellular mechanisms of the large and small dendritic activity. Dendritic Ca²⁺ activity can be caused by backpropagating action potentials (BPAPs) or local dendritic spikes; however, only the latter should be affected by glutamatergic blockers in the upper layers (Kondo et al., 2013). Moreover, it is known that dendritic spiking induces larger fluorescence changes in distal dendrites than that from BPAPs (Murayama et al., 2007, 2009). We therefore attributed CNQX-insensitive dendritic activity to BPAPs. To examine whether the large dendritic activity was due to dendritic Ca²⁺ spikes, we performed dendritic Ca²⁺ imaging before and after CNQX application to the cortical surface in S1 (Figures 5A and 5B). We used intracortical microstimulation (ICMS, 100 Hz 10 pulses) to M2 to mimic M2 activity (Figure 2), instead of hindpaw stimulation, because CNQX application to apical dendrites (or S1 cortical surface) of L5 neurons in vivo can block the early activity in S1 as seen in the cVSD imaging data (Figure 1) and multi-unit recording data (Figure S5G) which, in turn, would block activity in M2. The M2
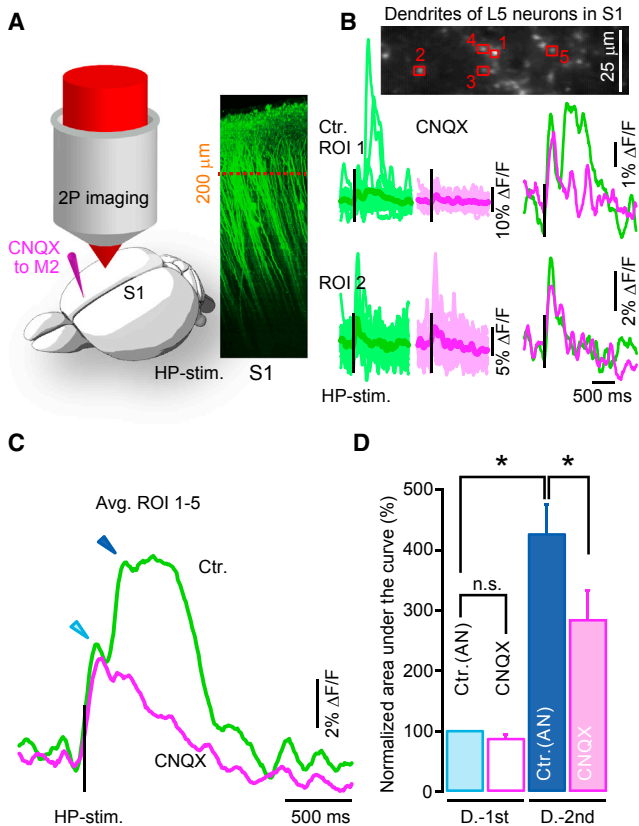
Figure 4. Top-Down Input Evokes Late Dendritic Ca²⁺ Signals in S1 L5 Neurons

(A) Experimental diagram of dendritic 2-photon Ca²⁺ imaging from S1 in the anesthetized mice with and without CNQX application to M2. Dendritic activity (measured 200 μm below the cortical surface) was evoked by hindpaw stimulation (single pulse, 0.1 ms duration, 100 V) in G-CaMP7 transgenic mice.

(B) Top, an example of an L5 neuron dendritic field imaged with a two-photon microscope. Five region of interests (ROIs) were evoked by the stimulation and marked (red boxes). Middle, dendritic activity in ROI 1 before (green) and after (pink) CNQX application to M2. The thin and thick traces show the activity for 30 trials and the averaged activity, respectively. Bottom, dendritic activity in ROI 2.

(C) Dendritic activity averaged in five ROIs. The light and deep blue arrowheads indicate the first (D.-1st) and second components (D.-2nd) of dendritic activity, respectively.

(D) Summary of (C) (n = 16 mice, 125 dendrites, $F_{(3, 60)}$ = 23.12, one-way ANOVA; D.-1st Ctr. and D.-1st CNQX, $F_{(4, 60)}$ = 0.017; D.-1st Ctr. and D.-2nd Ctr., $F_{(4, 60)}$ = 15.74; D.-2nd Ctr. and D.-2nd CNQX, $F_{(4, 60)}$ = 2.95, *p < 0.05, Scheffe's test). Data are represented as mean ± SEM.

ICMS evoked both small or large activity in different dendrites in S1 (Figures 5C, S6A, and S6B; see the Experimental Procedures for the categorization of dendritic activity). Notably, CNQX had a much larger effect on dendrites that had larger initial responses than on those with smaller initial responses (Figures 5C and 5D). CNQX application to the S1 cortical surface blocked M2 ICMS-evoked L2/3 and L5 firing activity in S1 (Figures S5F and S5G), indicating that ICMS evoked synaptic activity in S1 but not antidromic activation. Together, these data suggest that the small dendritic Ca²⁺ responses we observed in S1 arise from BPAPs,

while large responses are due to local dendritic Ca²⁺ spikes evoked by the M2 originated input to S1.

To further validate this conclusion, we studied small and large dendritic activity with another approach. It is known that distal dendrites of L5 neurons are inhibited by deep cortical interneurons (putative Martinotti cells) (Murayama et al., 2009). In an earlier study we showed that inhibition of the deep cortical layers (with either TTX or CNQX) leads to a paradoxical increase in dendritic Ca²⁺ activities due to release from dendritic inhibition. Here, we repeated the experiment to examine the effect of deep-layer interneuron activation on small and large dendritic Ca²⁺ activity by injecting CNQX into L5 of S1 during M2 ICMS (Figure 5E). With CNQX applied to L5, only the initially small dendritic Ca²⁺ responses were increased, with no significant change in the larger responses (Figures 5F, S6C, and S6D). As a control, the activation of deep layer interneurons in S1 could be evoked by hindpaw stimulation or M2 ICMS (Figure S7). These results suggest that small and large dendritic activity in L5 neurons is due to BPAPs and dendritic Ca²⁺ spikes, respectively, under control of S1 interneurons.

Accurate Sensory Perception Requires Top-Down Projection

Our results suggested that M2 regulates dendritic spiking in S1 L5 pyramidal neurons. We causally tested whether the M2 to S1 projection can influence somatosensory perception with optogenetic manipulation to inhibit axon terminals of the M2 fibers in S1 (Kitamura et al., 2014; Yamamoto et al., 2014). First, to ensure that we could reliably evoke and measure the optogenetic suppression of activity in M2 fibers projecting to S1, we locally expressed Archaerhodopsin (ArchT) (Han et al., 2011) in M2 neurons via viral infection with AAV-CMV-ArchT-EGFP (AAV-ArchT; see Figure S5H for injection site) and performed multiunit recordings with and without LED illumination of S1 during hindpaw stimulation (Figures 6A–6D). Light-induced inactivation of M2 fibers in S1 did not suppress the early component but did affect the late phase of L5 activity to ~70% of control (Figure 6C; see Figures S5K–S5M for other layers and for AAV-GFP-injected mice as a control experiment). Optogenetic inactivation of M2 fibers did not affect the membrane potential of M2 neurons (Figures S5I and S5J). In vivo patch-clamp recordings from L5 neurons confirmed that subthreshold slow responses following hindpaw stimulation were suppressed to ~70% of control during LED illumination of S1 (Figures 6E–6H). These findings provide confirmation and quantification of the strength and specificity of optogenetic inhibition of the M2-S1 projection.

To examine behaviors based on somatosensory perception, mice performed three different tasks: (1) spontaneous place preference test (SPPT), (2) stimulation-induced limb movement test (SILMT), and (3) tactile discrimination task (TDT). To specifically inactivate M2 fibers projecting to S1 during these behaviors, we injected AAV-ArchT into hindpaw M2 in both hemispheres (for SPPT and TDT) or in the right hemisphere (for SILMT) and employed a miniature LED illumination device mounted over hindpaw S1 through the skull (Figure 7A). We confirmed that almost no light from the LED bulb of the device reached M2 (Figure S8) and that the light to S1 did not affect somatic activity in M2, while direct illumination to M2 did
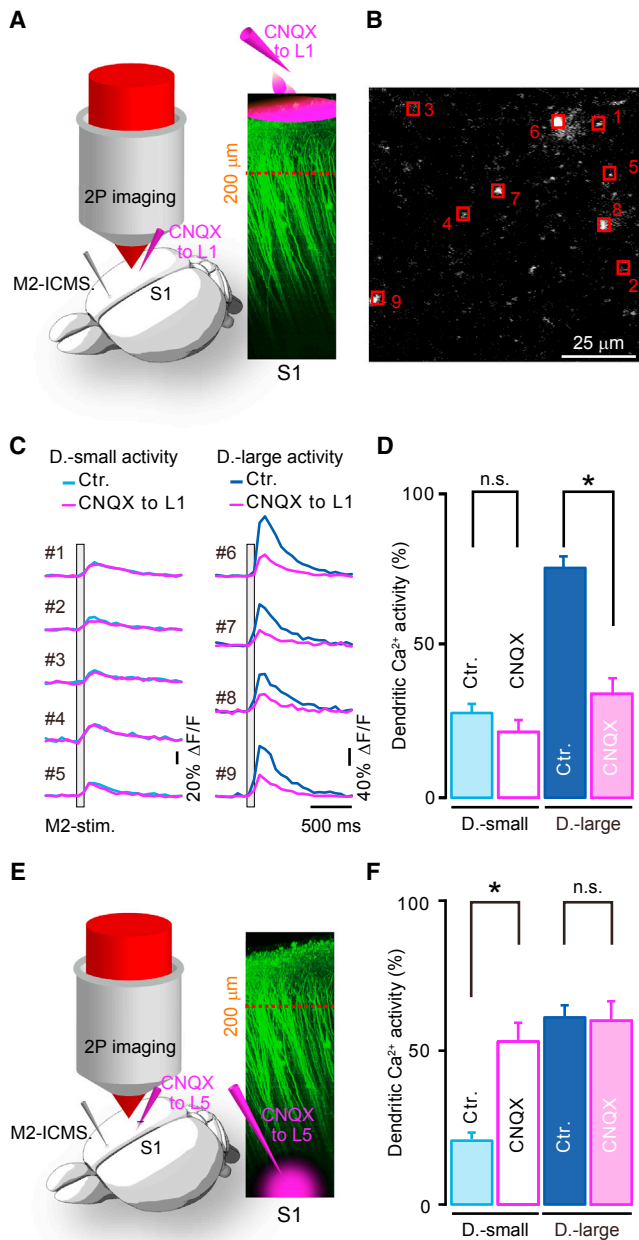
(Figure S9). In the SPPT (Figure 7B), whisker-trimmed mice could freely move and select their natural tactile preference in an open field square box containing two different textures (smooth and rough). Most (12 out of 15) control mice showed a clear innate texture preference for the rough surface, and the remainder (3 out of 15) preferred the smooth surface (Figure 7C). We quantified texture preference by recording the percent of cumulative time spent on the smooth or rough surface in both mouse groups and combined their preferences into a single data set. Control mice expressing GFP alone, or the experimental group expressing ArchT in the absence of LED illumination, also exhibited a strong texture preference. However, upon optogenetic bilateral (i.e., both hemispheres) inactivation of the projection from M2 to S1, texture preference in ArchT-expressing mice was eliminated, as observed by a reduction in time spent on the preferred texture (Figure 7D). These results indicate that sensory perception and/or preference for a particular texture depends on M2-mediated top-down control of S1.

Although we targeted AAV-ArchT injection to hindpaw M2 (the size of the injected area was ~750 μm diameter; Figure S5H), the AAV could in principle affect forepaw M2 that is ~900 μm away from hindpaw M2 (Figure S1C), to cause the behavioral changes. To examine this possibility, we performed SILMT by stimulating the contralateral forepaw or hindpaw with mild electrical stimulation in different trials, and then measured the movements of each limb (Figures 7E and 7F; see Experimental Procedures). The LED light was unilaterally (i.e., one side hemisphere) applied 50 ms after the stimulation for 450 ms to avoid the early sensory component of neural activity in S1 and selectively inactivate the late component. Limb movements were measured after the LED-on state for 1.0 s. We observed that M2 fiber inactivation at hindpaw S1 during the late component significantly reduced the probability of hindlimb movements (Figures 7G and 7H), and slightly reduced forelimb movements (p = 0.17) (see Table S1). These results indicate that hindpaw M2 axon inactivation at hindpaw S1 had little effect on forepaw perception and suggest that the M2-dependent late component in S1 is required for tactile perceptual behavior.

If sensory perception is affected by M2 fiber inactivation, other brain functions that are based on this perception must be also altered. In the TDT (Figures 7I and S10), mice with their whiskers trimmed were trained to discriminate between two different tactile stimuli randomly applied at track positions just before a Y branchpoint. Thus, the branchpoint decision was linked to texture discrimination in the maze. Bilateral optogenetic inactivation of the M2-S1 projection significantly inhibited correct performance in this task (see Figure 7J). The observed behavioral deficit in ArchT-injected mice was not caused by a motivational or attentional deficit, since there was no significant difference in the time that animals took to reach the texture nor in the time that they remained on the texture (Bushnell and Strupp, 2009) (Table S1). To examine whether this behavioral output was due to deficient sensory perception and not other factors such as decision-making, short-term memory, or behavioral asymmetry, we performed a conditioned alternation task (CAT). In the CAT (Figure 7K), mice were trained to choose each side arm alternately (i.e., one side arm first, then the other arm in the next trial, and so on). Optogenetic M2 fiber inactivation did not decrease the

Figure 5. M2 Stimulation Evokes Dendritic Spiking in S1 L5 Neurons
(A) Experimental diagram of CNQX application to S1 cortical surface under anesthesia. Dendritic Ca^{2+} activity was evoked by intracortical microstimulations (ICMS, L2/3, 0.2 mA, 1 ms duration, 10 pulses, 100 Hz) to M2 in G-CaMP7 transgenic mice.
(B) An example of dendrites of L5 neurons.
(C) Example of individual dendritic activity from the regions indicated in (B). See Figure S6 for dendritic activity categorization.
(D) Summary of activities in individual dendrites (n = 7 mice, D.-small, n = 23 dendrites, t_{22} = 1.64; D.-large, n = 25 dendrites, t_{24} = 8.29, *p < 0.01, Student's paired t test).
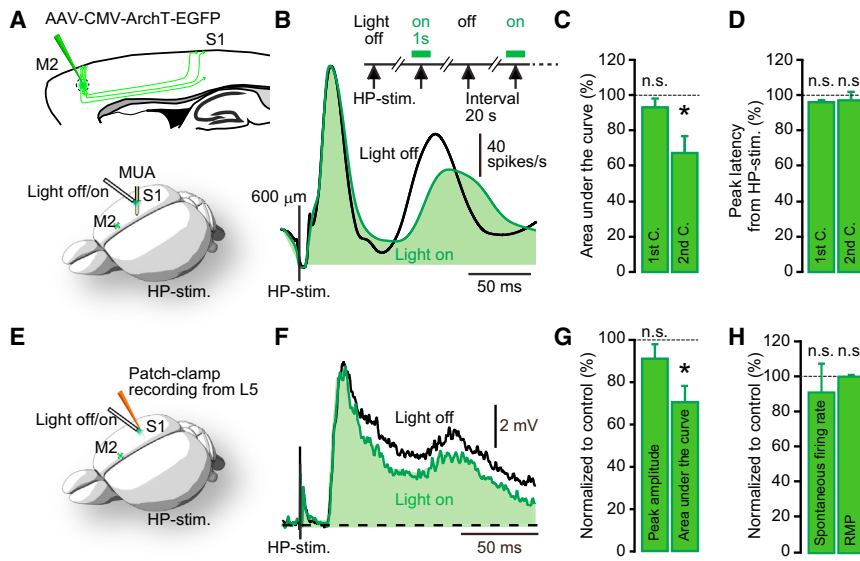(E) Experimental diagram of CNQX application to L5 neurons in the S1.
(F) Summary of the experiment (n = 6 mice, D.-small, n = 22 dendrites, t_{21} = 5.47; D.-large, n = 19 dendrites, t_{18} = 0.21, *p < 0.01, Student's paired t test, n.s., not significant). Data are represented as mean ± SEM.

Figure 6. Optogenetic Inactivation of Top-Down Input Suppressed S1 L5 Firing

(A) Experimental diagram of optogenetic inhibition of the projection from M2 to S1. Top, AAV-CMV-ArchT-EGFP was injected into M2 (see also Figure S5H for injection site and M2 axons). Bottom, MUA was recorded from S1, which was illuminated with green light to inactivate axons coming from M2. The firing activity was evoked by hindpaw stimulation (single pulse, 0.1 ms duration, 100 V).

(B) Example of the estimated spike rates at 600 μm below the cortical surface (L5) calculated from MUA is shown. MUA was evoked by hindpaw stimulation during light (LED)-off (black trace) and -on (green trace) conditions during anesthesia. Inset, timing of hindpaw stimulation and light illumination.

(C) Summary of the effect of LED illumination on the first and second components. The areas under the spike rate curves were measured and normalized to that recorded in the absence of LED illumination ($n = 9$ mice, 1st, $t_8 = -1.52$; 2nd, $t_8 = -3.89$, $*p < 0.02$, Student's paired t test; see also Figures S5K–S5M for other layers, and GFP experiments as control).

(D) The peak latencies of the spike rates from the hindpaw stimulation with and without LED illumination ($n = 9$ mice, 1st, $t_8 = -2.28$; 2nd, $t_8 = -0.63$, Student's paired t test).

(E) Experimental diagram showing whole-cell recording of membrane potential (Vm) in L5 pyramidal neurons of S1.

(F) Examples of averaged Vm (300 trials in each) evoked by a single hindpaw stimulation with (green) and without (black) LED illumination during anesthesia.

(G) Summary of the effects of LED illumination on the peak amplitude and the area under the Vm curve evoked by hindpaw stimulation ($n = 7$ mice, peak amplitude, $t_{12} = 1.36$; the area under the Vm curve, $t_{12} = 3.78$, $*p < 0.01$, Student's t test).

(H) Summary of the effect of LED illumination on the spontaneous firing rate and resting membrane potential (RMP) ($n = 7$ mice, spontaneous firing rate, $t_{12} = 0.54$; RMP, $t_{12} = 0.63$, Student's t test). Data are represented as mean ± SEM; n.s., not significant.

success rate in this task (Figure 7L), which would otherwise have indicated deficient perception. Therefore, the mice in the TDT simply failed to recognize an accurate texture when the M2 to S1 projection was inhibited.

Together, the SPPT, SILMT, and TDT behavioral results support the hypothesis that sensory perception and/or preference for texture somatosensation via their hindpaws were inaccurate during inactivation of the M2 top-down input to S1. We also performed an extensive battery of control behaviors during optogenetic manipulation to rule out spurious effects of M2 top-down input on normal visual perception, motor function, anxiety, and acute pain in tests that included the open field test, gait analysis during treadmill walking, and a hot plate test with whisker-trimmed mice (Table S1). Together, these behavioral findings demonstrate that the M2 top-down projection to the S1 tactile region is required for accurate sensory perception in awake-behaving mice.

DISCUSSION

In this study, we characterized a neural circuit for top-down control in mouse somatosensory cortex, including its physiological mechanism and role in sensory perception. L5 pyramidal neurons are hypothesized to be associative elements for the coincident detection of bottom-up and top-down inputs (Felleman and Van Essen, 1991; Gilbert and Sigman, 2007; Larkum, 2013; Larkum et al., 1999). In this study, we confirmed that thalamic and M2 top-down inputs converge in S1, but we found that the association could be divided into discrete early (bottom-up) and late (top-down) temporal components. In the late component, M2 triggered the S1 cortical column from lower to upper layers for dendritic spiking and robust firing of L5 pyramidal neurons.

Primary sensory cortex has been hypothesized to receive top-down information in the late activity component to generate conscious perception (Cauller, 1995; Gilbert and Sigman, 2007; Lamme, 2001; Meyer, 2011; Sachidhanandam et al., 2013; Supèr et al., 2001). One proposed mechanism for late component activation with support in vitro (Larkum et al., 1999) and in vivo (Xu et al., 2012) is that coincident activation of bottom-up and top-down inputs trigger back-propagating action-potential-activated calcium spike (BAC) firing (Larkum, 2013). For this mechanism to apply, top-down and bottom-up inputs to apical dendrites in primary sensory cortex must converge within a 30 ms time window (Ledergerber and Larkum, 2012). However, in the majority of sensory processing, top-down input reaches primary sensory cortex long after (50–150 ms) the arrival of bottom-up sensory information. On the other hand, our data suggest that it is hypothetically possible that the BAC firing mechanism can be triggered by the top-down projection from M2 alone, without required bottom-up input convergence, because M2 axons terminate in both S1 L1 and L6 (Figure S11). Consistent with this hypothesis, we observed synaptic inputs (sinks in the CSD analysis) at depths of 200 and 800 μm with average overlap periods of ~30 ms (Figure S5E). Within this overlap period, L5 neurons can probabilistically integrate inputs to basal dendrites first and distal dendrites in a late phase, or vice versa, to produce a L5 dendritic spike (Ledergerber and
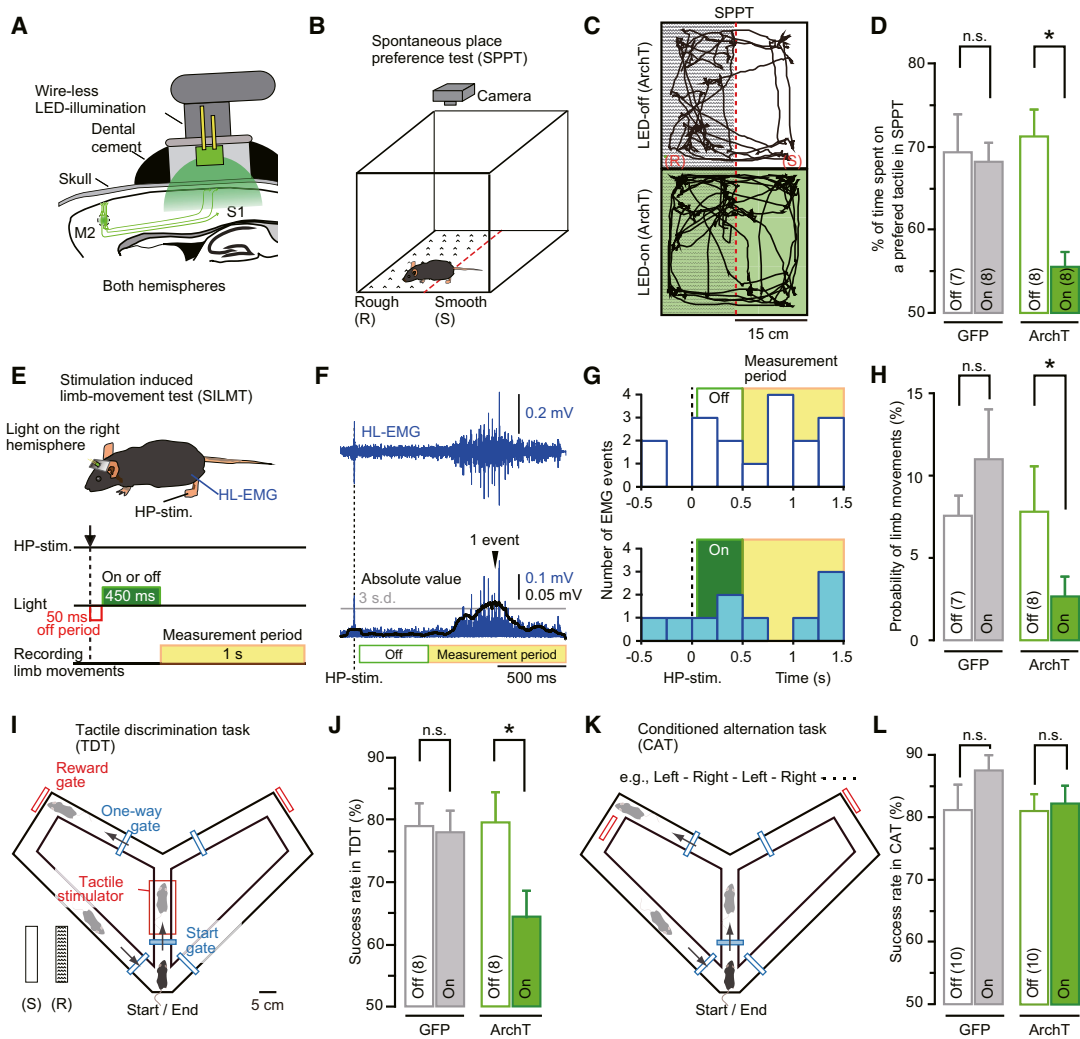
Figure 7. Optogenetic Inactivation of Top-Down Input Alters Sensory Perception

(A) Experimental diagram of a miniature wireless LED device attached to the S1 in the both hemispheres. AAV-ArchT or GFP was also injected to M2 in the both hemispheres. A sagittal image is shown.

(B) Diagram showing the mouse behavioral setup for the spontaneous place preference test (SPPT).

(C) Place preference location plots from two representative ArchT injected mice showing the animal's position over the course of the 4 min session with and without LED illumination.

(D) Summary of the preference in the SPPT. Two-way ANOVA revealed a significant interaction effect of injection substrate (GFP or ArchT) and LED (on or off) ($F_{(1, 27)}$ = 5.29, p < 0.05), and a post hoc test revealed a significant of LED effect on ArchT group (LED-off, 71.2% ± 3.3% versus LED-on, 55.7% ± 1.8%, $F_{(1, 27)}$ = 12.94, *p < 0.01).

(E) Experimental diagram of stimulation induced limb movement test (SILMT). Contralateral hindpaw stimulation (single pulse, 0.1 ms duration, 1.0 mA) was applied and LED light (450 ms duration) was applied 50 ms after the stimulation.

(F) Example of EMG recording during hindpaw stimulation without LED illumination.

(G) Example of detected hindlimb movements (see Experimental Procedures) during LED-off state (top) and on state (bottom) in an AAV-ArchT injected mouse.

(H) Summary of (G) in ArchT and GFP injected mice. Two-way repeated-measures ANOVA revealed a significant interaction effect of injection substrate (GFP or ArchT) and LED (on or off) ($F_{(1, 14)}$ = 7.08, p < 0.05), and a post hoc test revealed a significant of LED effect on ArchT group ($F_{(1, 14)}$ = 5.1, p < 0.05). See also Table S1 for forelimb movements.

(I) Diagrams of mouse behavior in the tactile discrimination task (TDT). See Figure S10 for additional details. M2 fibers were optogenetically inactivated in both hemispheres likewise (A).

(J) Summary of the success rate in the TDT. Two-way repeated-measures ANOVA revealed a significant interaction effect of injection substrate (GFP or ArchT) and LED (on or off) ($F_{(1, 14)}$ = 4.82, p < 0.05), and a post hoc test revealed a significant of LED effect on ArchT group (LED-off, 79.5% ± 5.0% versus LED-on, 64.5% ± 4.2%, $F_{(1, 14)}$ = 9.78, *p < 0.01).

(K) Diagrams of mouse behavior in the conditioned alternation task (CAT).

(L) Summary of the CAT success rate. No significant main and interaction effect were found with two-way repeated-measures ANOVA. Data are represented as mean ± SEM; n.s., not significant. The numbers in parentheses in each graph show the number of mice used in each experiment.
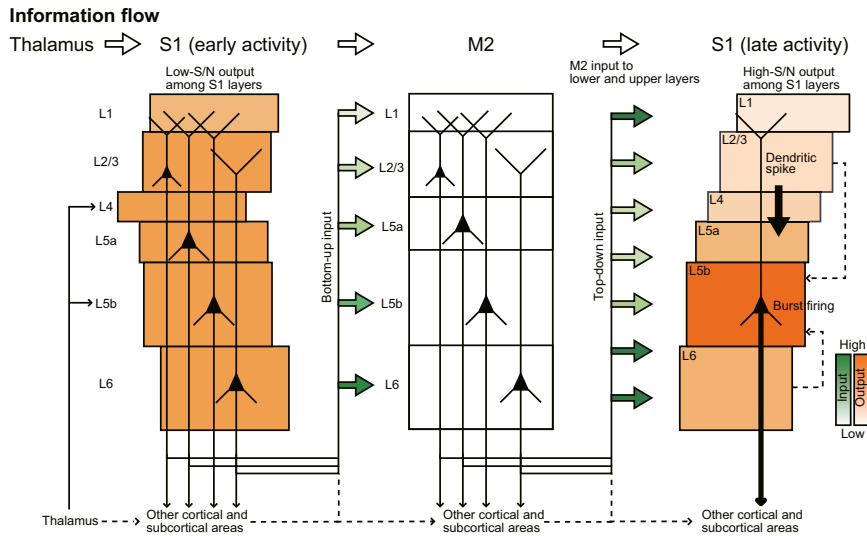
Information flow

Figure 8. Diagram of a Top-Down Signal Processing Circuit for Sensory Perception
Summary of the top-down control circuit between M2 and S1. Sensory thalamic inputs arrive at S1 and recruit neurons uniformly across all layers, creating a low-contrast early bottom-up output from S1 to M2. Neurons in L2/3, L5a, and L6 of S1 project their axons to all layers of M2. From M2, neurons in L2/3, L6, and L5a project axons preferentially to the deep and upper layers of S1. These M2 inputs reach at S1, which drives dendritic spike and burst firing in L5b neurons, resulting in higher activity to other layers. See also Figure S11.

Larkum, 2012). The axonal pattern of innervation by top-down input is ubiquitous across the cortex (Felleman and Van Essen, 1991), suggesting that this form of top-down connectivity might operate throughout cortex to maintain top-down activation of L5 pyramidal neurons. The M2-S1 top-down input that we observed is qualitatively different from conventionally described top-down inputs for cognitive priorities like attention, expectation, motivation, or memory, that are internally generated and transmitted from higher-order to lower sensory areas (Figure S11). Due to M2's direct activation of L5 dendrites in the absence of temporal coincidence with a bottom-up input, we propose that the M2-S1 neural circuit may serve as a safety mechanism to enable reliable, accurate, and continuous sensory perception without internally generated top-down inputs. This class of sensory-type top-down circuit would operate in parallel with conventional cognitive-type top-down circuits, but further investigation is required to validate this hypothesis.

The M2 to S1 neural circuit is summarized in Figure 8. In this model, sensory information travels to S1 from thalamus, which then relays the early phase of output to other brain areas, including M2 (Figure 1). Next, top-down input from M2 to S1 triggers a second (late) phase of output (Figure 2). Activation of the S1 cortical column in the early and late phases is layer dependent (Figure 2); in the early phase, the circuit processes simple features of the sensory stimulus, resulting in uniform activity in neurons of all layers to generate a low signal-to-noise (S/N) cortical output from all layers (Figure 2) that is transmitted to other areas including M2. This information is then returned from M2 to S1 via the recurrent top-down projection (Figure 2) to both the upper and lower layers of the S1 column (Figure 3), resulting in increased dendritic spiking in L5 neurons (Figure 4) and a second component as high S/N cortical output (Figure 2). Also, L2/3 and L6 neurons and inhibitory neurons may contribute to the robust firing activity of L5 neurons. M2 input can also trigger the firing of deep layer Martinotti-type interneurons (Figures 5 and S7), which can inhibit the dendritic spike in L5 neurons (Murayama et al., 2009). Thus, the M2 projections to S1 contains multiple, parallel pathways to refine L5 synaptic activity.

While our findings support a direct corticocortical connection between M2 and S1, we do not exclude the involvement of additional indirect pathways to M2 via the thalamus (Ueta et al., 2013) and other cortical areas. For instance, M1 also projects to S1 with a similar pattern of axonal terminations (Matyas et al., 2010), and the projection to S1 L1 profoundly influences Ca^{2+} in L5 pyramidal neuron distal dendrites (Xu et al., 2012). Since M1 is also activated by M2 (Ueta et al., 2013), it remains possible that M2 could project to S1 indirectly via M1. We include these putative indirect pathways in Figure 8. It should be noted, however, that our optogenetic inactivation of M2 fibers in S1 showed negligible deficits in M1-based motor behavior but instead demonstrate a role for the M2-S1 top-down connection in sensory perception.

Regarding our findings on the effect of optogenetic inhibition of M2 axons in S1 on somatosensory perception, we can only infer what mice experience based on their overt decision-making, and therefore our behavioral findings must be interpreted with caution. However, in the three different behavioral tasks we used to examine somatosensory tactile perception on the paws, the LED-on mice showed remarkable alterations in sensory function. The most plausible explanation of these findings is that the mice experienced either absent or fictive perception of tactile surfaces in the tasks resulting in inaccurate judgment of the sensory input. These overall conclusions are consistent with a human study using transcranial magnetic stimulation (Wokke et al., 2013) where feedback to early sensory areas contributed to veridical perception as subjects reported subjective fictive perception during the stimulation. Therefore, the mouse behaviors during functional inactivation of the M2 to S1 projection are consistent with a switch from accurate to inaccurate sensory perception. The findings imply that top-down control, at least for the M2 to S1 circuit we describe, is an intrinsic component involved in the direct sensory perception of tactile stimuli to the paws.

As discussed in the Introduction, the sensory stimulus-evoked late component neuronal activity in primary sensory cortex is hypothesized to be associated with conscious awareness of the stimulus (Cauller and Kulics, 1991; Supèr et al., 2001). For example, Dehaene and colleagues (Dehaene and Changeux, 2005; Dehaene et al., 2003) have proposed models in which the level of conscious perception can be estimated from the

late component activity. It is tempting to speculate that the late activity component we observe in our studies may be responsible for conscious sensory perception. In the SILMT, the probability of hindpaw movement decreased (Figures 7G and 7H) with optogenetic inactivation during the late component, and sensory perception and animal movement was suppressed by optogenetic inactivation, consistent with the interpretation that the late component activity in S1, which we showed involves regenerative dendritic spiking and S1 L5 persistent neuron firing, is necessary for sensory perception of the stimulus. We showed that the M2 to S1 top-down connection drives L5 dendritic spiking during the late component, and that this is required for accurate tactile sensory perception. However, definitive evidence for the role of this neural circuit in conscious perception would require manipulation of L5 activity in vivo.

EXPERIMENTAL PROCEDURES

Wild-type (C57BL/6JJmsSlc) mice, G-CaMP7 transgenic mice, and GAD67-GFP knock-in mice were used. The animals' ages were older than postnatal day 28 (P28). Animals were anesthetized with isoflurane (1%–2%, vol/vol). The voltage-sensitive dye (VSD) RH1691 was applied to the cortex. The fluorescence of the VSD was collected by a high-speed CMOS camera (Brainvision). In vivo whole-cell recordings from L5 pyramidal neurons were made with a "blind" patch-clamp recording technique. A Pipette (5–8 MΩ) was filled with intracellular solution composed of (in mM) 135 K-gluconate, 4 KCl, 10 HEPES, 10 Na_2-phosphocreatine, 4 Mg-ATP, 0.3 Na-GTP, and 20 μM Alexa Fluor 594 hydrazide sodium salt (Alexa594) and had a pH of 7.2 (adjusted with KOH) and osmolarity of 300 mOsm. The G-CaMP7 transgenic mice were used for in vivo dendritic Ca^{2+} imaging from L5 pyramidal neurons with a custom-modified multiphoton microscope (Nikon Corporation, Tokyo, Japan). Silicon probes with a single shank (NeuroNexus) containing 16 recording sites were used to simultaneously sample LFP and MUA. Each probe site was a circle, 30 μm in diameter, which was separated vertically by 100 μm and had impedances of 0.3–0.8 MΩ at 1 kHz. Ag/AgCl wires were used as a reference electrode and were set on a chamber that was placed on the skull. AAV-CMV-ArchT-EGFP or AAV-CAG-GFP (~300 nl) was pressure injected into M2 two to three times (for ~30 min in each). Physiological and behavioral experiments were performed 4–8 weeks after the injection. For behavioral experiments, the bilateral M2 of wild-type mice were injected with the virus, and then a custom-made wireless LED illumination device (Bio Research Center, Aichi, Japan) was attached to the skull over the S1 area. Mice were randomly assigned to the experimental and control groups at the beginning of the experiments (e.g., before virus infection). Although data collection and statistical analyses were not performed blindly (e.g., repeated treatment and trials), automated experimental apparatuses and data analyzing software should minimize biases due to experimental procedures. For physiological experiments, statistical analyses were performed using Microsoft Excel (Microsoft, Redmond, WA, USA) Matlab 2013 (MathWorks Inc., Natick, MA, USA) or Igor Pro (WaveMetrics, Portland, OR, USA) software programs. For behavioral experiments, statistical analyses were performed with SPSS software version 17 (SPSS Inc., Chicago, IL, USA). Additional information can be found in Supplemental Experimental Procedures.

SUPPLEMENTAL INFORMATION

Supplemental Information includes 11 figures, one table, and Supplemental Experimental Procedures and can be found with this article at http://dx.doi.org/10.1016/j.neuron.2015.05.006.

AUTHOR CONTRIBUTIONS

M.M. designed the study. S.M. performed the in vivo two-photon dendritic imaging and somatic patch-clamp and targeted-cell attached recordings. T.S. performed the cVSD imaging. T.M. performed the multiunit recordings. K.O. analyzed the firing data. T.M. and K.O. performed current source density (CSD) analysis. C.H., K.Y., and S.M. performed behavioral tests and analyses. A.I. and A.Y. generated AAV-CMV-ArchT-EGFP vector. M.O. performed the anatomical studies and viral injections. C.M. contributed breeding and genotyping of the mouse colony and producing AAV stocks. M.O. and J.N. generated the G-CaMP7-T2A-DsRed2 transgene. M.S. and Y.H. made the Thy1-G-CaMP7-T2A-DsRed2 transgenic mouse line. Y.Y. generated the GAD67-GFP knockin mice. M.M., M.E.L., and S.M. prepared the manuscript. All authors contributed to the discussion on the experimental procedures, the results, and the manuscript.

ACKNOWLEDGMENTS

REFERENCES

Armstrong-James, M., Fox, K., and Das-Gupta, A. (1992). Flow of excitation within rat barrel cortex on striking a single vibrissa. J. Neurophysiol. 68, 1345–1358.

Ayling, O.G., Harrison, T.C., Boyd, J.D., Goroshkov, A., and Murphy, T.H. (2009). Automated light-based mapping of motor cortex by photoactivation of channelrhodopsin-2 transgenic mice. Nat. Methods 6, 219–224.

Bushnell, P.J., and Strupp, B.J. (2009). Assessing attention in rodents. In Methods of Behavior Analysis in Neuroscience, J.J. Buccafusco, ed. (Boca Raton, FL: CRC Press).

Cauller, L. (1995). Layer I of primary sensory neocortex: where top-down converges upon bottom-up. Behav. Brain Res. 71, 163–170.

Cauller, L.J., and Kulics, A.T. (1988). A comparison of awake and sleeping cortical states by analysis of the somatosensory-evoked response of postcentral area 1 in rhesus monkey. Exp. Brain Res. 72, 584–592.

Cauller, L.J., and Kulics, A.T. (1991). The neural basis of the behaviorally relevant N1 component of the somatosensory-evoked potential in SI cortex of awake monkeys: evidence that backward cortical projections signal conscious touch sensation. Exp. Brain Res. 84, 607–619.

Cauller, L.J., Clancy, B., and Connors, B.W. (1998). Backward cortical projections to primary somatosensory cortex in rats extend long horizontal axons in layer I. J. Comp. Neurol. *390*, 297–310.

Constantinople, C.M., and Bruno, R.M. (2013). Deep cortical layers are activated directly by thalamus. Science *340*, 1591–1594.

Coogan, T.A., and Burkhalter, A. (1990). Conserved patterns of cortico-cortical connections define areal hierarchy in rat visual cortex. Exp. Brain Res. *80*, 49–53.

Corbetta, M., and Shulman, G.L. (2002). Control of goal-directed and stimulus-driven attention in the brain. Nat. Rev. Neurosci. *3*, 201–215.

Dehaene, S., and Changeux, J.P. (2005). Ongoing spontaneous activity controls access to consciousness: a neuronal model for inattentional blindness. PLoS Biol. *3*, e141.

Dehaene, S., Sergent, C., and Changeux, J.P. (2003). A neuronal network model linking subjective reports and objective physiological data during conscious perception. Proc. Natl. Acad. Sci. USA *100*, 8520–8525.

Dehaene, S., Changeux, J.P., Naccache, L., Sackur, J., and Sergent, C. (2006). Conscious, preconscious, and subliminal processing: a testable taxonomy. Trends Cogn. Sci. *10*, 204–211.

Del Cul, A., Baillet, S., and Dehaene, S. (2007). Brain dynamics underlying the nonlinear threshold for access to consciousness. PLoS Biol. *5*, e260.

Felleman, D.J., and Van Essen, D.C. (1991). Distributed hierarchical processing in the primate cerebral cortex. Cereb. Cortex *1*, 1–47.

Ferezou, I., Haiss, F., Gentet, L.J., Aronoff, R., Weber, B., and Petersen, C.C. (2007). Spatiotemporal dynamics of cortical sensorimotor integration in behaving mice. Neuron *56*, 907–923.

Gilbert, C.D., and Sigman, M. (2007). Brain states: top-down influences in sensory processing. Neuron *54*, 677–696.

Han, X., Chow, B.Y., Zhou, H., Klapoetke, N.C., Chuong, A., Rajimehr, R., Yang, A., Baratta, M.V., Winkle, J., Desimone, R., and Boyden, E.S. (2011). A high-light sensitivity optical neural silencer: development and application to optogenetic control of non-human primate cortex. Front. Syst. Neurosci. *5*, 18.

Johnson, R.R., and Burkhalter, A. (1996). Microcircuitry of forward and feedback connections within rat visual cortex. J. Comp. Neurol. *368*, 383–398.

Kitamura, T., Pignatelli, M., Suh, J., Kohara, K., Yoshiki, A., Abe, K., and Tonegawa, S. (2014). Island cells control temporal association memory. Science *343*, 896–901.

Kondo, M., Kitajima, T., Fujii, S., Tsukada, M., and Aihara, T. (2013). Modulation of synaptic plasticity by the coactivation of spatially distinct synaptic inputs in rat hippocampal CA1 apical dendrites. Brain Res. *1526*, 1–14.

Kulics, A.T. (1982). Cortical neural evoked correlates of somatosensory stimulus detection in the rhesus monkey. Electroencephalogr. Clin. Neurophysiol. *53*, 78–93.

Kulics, A.T., Lineberry, C.G., and Roppolo, J.R. (1977). Neurophysiological correlates of sensory discrimination performance to electrical cutaneous stimuli in rhesus monkey. Brain Res. *136*, 360–365.

Lamme, V.A. (2001). Blindsight: the role of feedforward and feedback cortico-cortical connections. Acta Psychol. (Amst.) *107*, 209–228.

Larkum, M. (2013). A cellular mechanism for cortical associations: an organizing principle for the cerebral cortex. Trends Neurosci. *36*, 141–151.

Larkum, M.E., Zhu, J.J., and Sakmann, B. (1999). A new cellular mechanism for coupling inputs arriving at different cortical layers. Nature *398*, 338–341.

Ledergerber, D., and Larkum, M.E. (2012). The time window for generation of dendritic spikes by coincidence of action potentials and EPSPs is layer specific in somatosensory cortex. PLoS ONE *7*, e33146.

Matyas, F., Sreenivasan, V., Marbach, F., Wacongne, C., Barsy, B., Mateo, C., Aronoff, R., and Petersen, C.C. (2010). Motor control by sensory cortex. Science *330*, 1240–1243.

Mesulam, M.M. (1998). From sensation to cognition. Brain *121*, 1013–1052.

Meyer, K. (2011). Primary sensory cortices, top-down projections and conscious experience. Prog. Neurobiol. *94*, 408–417.

Milenkovic, N., Zhao, W.J., Walcher, J., Albert, T., Siemens, J., Lewin, G.R., and Poulet, J.F. (2014). A somatosensory circuit for cooling perception in mice. Nat. Neurosci. *17*, 1560–1566.

Miller, E.K., and Cohen, J.D. (2001). An integrative theory of prefrontal cortex function. Annu. Rev. Neurosci. *24*, 167–202.

Murakami, M., Vicente, M.I., Costa, G.M., and Mainen, Z.F. (2014). Neural antecedents of self-initiated actions in secondary motor cortex. Nat. Neurosci. *17*, 1574–1582.

Murayama, M., Pérez-Garci, E., Lüscher, H.R., and Larkum, M.E. (2007). Fiberoptic system for recording dendritic calcium signals in layer 5 neocortical pyramidal cells in freely moving rats. J. Neurophysiol. *98*, 1791–1805.

Murayama, M., Pérez-Garci, E., Nevian, T., Bock, T., Senn, W., and Larkum, M.E. (2009). Dendritic encoding of sensory stimuli controlled by deep cortical interneurons. Nature *457*, 1137–1141.

Neafsey, E.J., Bold, E.L., Haas, G., Hurley-Gius, K.M., Quirk, G., Sievert, C.F., and Terreberry, R.R. (1986). The organization of the rat motor cortex: a microstimulation mapping study. Brain Res. *396*, 77–96.

Ohkura, M., Sasaki, T., Sadakari, J., Gengyo-Ando, K., Kagawa-Nagamura, Y., Kobayashi, C., Ikegaya, Y., and Nakai, J. (2012). Genetically encoded green fluorescent Ca2+ indicators with improved detectability for neuronal Ca2+ signals. PLoS ONE *7*, e51286.

Olson, I.R., Chun, M.M., and Allison, T. (2001). Contextual guidance of attention: human intracranial event-related potential evidence for feedback modulation in anatomically early temporally late stages of visual processing. Brain *124*, 1417–1425.

Paxinos, G., and Watson, C. (1998). The Rat Brain in Stereotaxic Coordinates (San Diego: Academic Press).

Petreanu, L., Gutnisky, D.A., Huber, D., Xu, N.L., O'Connor, D.H., Tian, L., Looger, L., and Svoboda, K. (2012). Activity in motor-sensory projections reveals distributed coding in somatosensation. Nature *489*, 299–303.

Reep, R.L., Corwin, J.V., Hashimoto, A., and Watson, R.T. (1984). Afferent connections of medial precentral cortex in the rat. Neurosci. Lett. *44*, 247–252.

Reep, R.L., Corwin, J.V., Hashimoto, A., and Watson, R.T. (1987). Efferent connections of the rostral portion of medial agranular cortex in rats. Brain Res. Bull. *19*, 203–221.

Reep, R.L., Goodwin, G.S., and Corwin, J.V. (1990). Topographic organization in the corticocortical connections of medial agranular cortex in rats. J. Comp. Neurol. *294*, 262–280.

Rubio-Garrido, P., Pérez-de-Manzo, F., Porrero, C., Galazo, M.J., and Clascá, F. (2009). Thalamic input to distal apical dendrites in neocortical layer 1 is massive and highly convergent. Cereb. Cortex *19*, 2380–2395.

Sachidhanandam, S., Sreenivasan, V., Kyriakatos, A., Kremer, Y., and Petersen, C.C. (2013). Membrane potential correlates of sensory perception in mouse barrel cortex. Nat. Neurosci. *16*, 1671–1677.

Sato, M., Mizuta, K., Kawano, M., Takekawa, T., Islam, T., Yamakawa, H., Yamaguchi, Y., Fukai, T., Ohkura, M., Nakai, J., and Hayashi, Y. (2013). Hippocampal CA1 network dynamics during locomotion in virtual reality. Soc. Neurosci. Abstr. 770.10.

Schneider, D.M., Nelson, A., and Mooney, R. (2014). A synaptic and circuit basis for corollary discharge in the auditory cortex. Nature *513*, 189–194.

Sul, J.H., Jo, S., Lee, D., and Jung, M.W. (2011). Role of rodent secondary motor cortex in value-based action selection. Nat. Neurosci. *14*, 1202–1208.

Supèr, H., Spekreijse, H., and Lamme, V.A. (2001). Two distinct modes of sensory processing observed in monkey primary visual cortex (V1). Nat. Neurosci. *4*, 304–310.

Tamamaki, N., Yanagawa, Y., Tomioka, R., Miyazaki, J., Obata, K., and Kaneko, T. (2003). Green fluorescent protein expression and colocalization with calretinin, parvalbumin, and somatostatin in the GAD67-GFP knock-in mouse. J. Comp. Neurol. *467*, 60–79.

Tomita, H., Ohbayashi, M., Nakahara, K., Hasegawa, I., and Miyashita, Y. (1999). Top-down signal from prefrontal cortex in executive control of memory retrieval. Nature *401*, 699–703.

Ueta, Y., Otsuka, T., Morishima, M., Ushimaru, M., and Kawaguchi, Y. (2013). Multiple layer 5 pyramidal cell subtypes relay cortical feedback from secondary to primary motor areas in rats. Cereb. Cortex *24*, 2362–2376.

Vargo, J.M., Corwin, J.V., King, V., and Reep, R.L. (1988). Hemispheric asymmetry in neglect produced by unilateral lesions of dorsomedial prefrontal cortex in rats. Exp. Neurol. *102*, 199–209.

Wokke, M.E., Vandenbroucke, A.R., Scholte, H.S., and Lamme, V.A. (2013). Confuse your illusion: feedback to early visual cortex contributes to perceptual completion. Psychol. Sci. *24*, 63–71.

Xu, N.L., Harnett, M.T., Williams, S.R., Huber, D., O'Connor, D.H., Svoboda, K., and Magee, J.C. (2012). Nonlinear dendritic integration of sensory and motor input during an active sensing task. Nature *492*, 247–251.

Yamamoto, J., Suh, J., Takeuchi, D., and Tonegawa, S. (2014). Successful execution of working memory linked to synchronized high-frequency gamma oscillations. Cell *157*, 845–857.

Zanto, T.P., Rubens, M.T., Thangavel, A., and Gazzaley, A. (2011). Causal role of the prefrontal cortex in top-down modulation of visual processing and working memory. Nat. Neurosci. *14*, 656–661.